# HIGH RESOLUTION ISOTOPE SCLEROCHRONOLOGY REFLECTS SEASONAL CYCLE CHANGES AT ROCKY POINT, BELIZE BETWEEN THE LAST INTERGLACIAL AND PRESENT

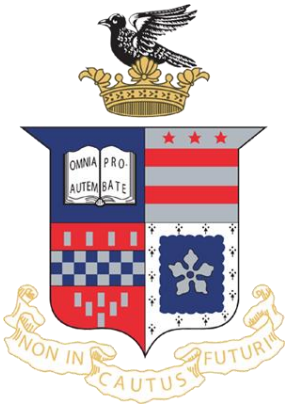


**Hayden R. Yates**

**Dr. Lisa Greer, Faculty Advisor**

**Washington and Lee University**

**Senior Thesis**

**April 2016**

## Table of Contents

**List of Figures** ... 3
**List of Tables** ... 3
**Acknowledgements** ... 4
**Abstract** ... 5
**I.** Introduction ... 6
**1.** Pleistocene Climate ... 6
**2.** Milankovitch Cycles ... 7
**3.** Intertropical Convergence Zone ... 8
**4.** Coral Sclerochronology ... 9
**5.** Stable Isotopes ... 10
**5.1.** Carbon Isotopes ... 10
**5.2.** Oxygen Isotopes ... 11
**II.** Study Locality ... 13
**III.** Methodology ... 15
**IV.** Results ... 20
**1.** Linear Extension Rates ... 21
**2.** External Calibration ... 21
**3.** Sampling Resolution ... 21
**3.1.** Oxygen ... 21
**3.2.** Carbon ... 23
**4.** Stable Isotope Transects ... 24
**4.1.** Bulk Isotopic Signatures ... 24
**4.2.** Seasonal Ranges ... 25
**V.** Discussion ... 30
**VI.** Conclusions ... 35
**VII.** References ... 36

## List of Figures

**1.** Annual Insolation Variability at 18°N: Pleistocene vs. Modern ..... 8
**2.** Spatial Variation of the ITCZ on a seasonal time scale ..... 9
**3.** Map of Study Location: Belize ..... 14
**4A.** Coral Slab BZRP12 ..... 15
**4B.** Composite Coral X-radiograph BZRP12 ..... 15
**5.** Sampling Resolution X-Radiograph BZRP12 ..... 17
**6.** Linear Extension Rates Box Plot ..... 20
**7A.** $\delta^{18}O$ Pleistocene Coral Sampling Resolution BZRP12 ..... 22
**7B.** $\delta^{18}O$ Modern Coral Sampling Resolution BZ14RP ..... 22
**8A.** $\delta^{13}C$ Pleistocene Coral Sampling Resolution BZRP12 ..... 23
**8B.** $\delta^{13}C$ Modern Coral Sampling Resolution BZ14RP ..... 24
**9A.** $\delta^{13}C$ Bulk Population Box Plot ..... 25
**9B.** $\delta^{18}O$ Bulk Population Box Plot ..... 25
**10.** $\delta^{18}O$ Pleistocene Coral BZRP12 ..... 26
**11.** $\delta^{18}O$ Pleistocene Coral BZRP14 ..... 27
**12.** $\delta^{18}O$ Modern Coral BZ14RP ..... 27
**13.** $\delta^{13}C$ Pleistocene Coral BZRP12 ..... 28
**14.** $\delta^{13}C$ Pleistocene Coral BZRP14 ..... 28
**15.** $\delta^{13}C$ Modern Coral BZ14RP ..... 29

## List of Tables

**1.** Linear Extension Rates ..... 20
**2.** Sampling Resolution Isotopic Means and Seasonal Ranges ..... 21
**3.** Bulk Population Isotopic Means and Variability ..... 24
**4.** Annually Resolved Seasonal Ranges ..... 26

**Acknowledgements**

First and foremost, I would like to thank my advisor Dr. Lisa Greer, for her guidance throughout this entire project. My thesis would not have been possible without her, and I am fortunate to have had the opportunity to work with her. I have learned so much from her during this entire process, and I genuinely appreciate all of the time and effort that she has dedicated to me. This has been such a formative experience and I owe her many thanks for that. Additionally, I would like to thank Emily Falls for her tireless assistance and support, especially regarding the Washington and Lee stable isotope ratio mass spectrometer. Emily's contributions to my thesis have been immeasurable and I would not have been able to do it without her.

I would also like to acknowledge and thank Ilian DeCorte, for his collaborative efforts. Without Ilian, my thesis would only be half of what it is today. Thank you to Dr. Jill Leonard-Pingel for her guidance. Thank you to Dr. Omar Paredes for assisting with the x-radiographs of my coral slabs and Dr. Tara Clark for generating $^{230}Th/^{234}U$ dates for two of my samples. Finally, I am grateful to the Washington and Lee Geology Department for funding support via the R. Preston Hawkins IV award and for general support throughout my college career.

**Abstract**

The last Pleistocene interglacial period is thought to be characterized by warmer temperatures, higher precipitation, higher sea level and lower ice volume than today due to different orbital forcing parameters at that time. During the last interglacial, elliptical eccentricity, pronounced obliquity, and minimal precession perpetuated changes in solar insolation distribution in the Northern Hemisphere, specifically by creating a stronger summer insolation and a weakened winter insolation. In this study, $\delta^{18}O$ and $\delta^{13}C$ isotopic records were used to investigate the impacts of solar variability on tropical Caribbean seasonality at the last interglacial. Growth rate and stable isotope data were obtained from two Pleistocene corals (BZRP12 and BZRP14) from Rocky Point, Belize and two modern corals from Rocky Point, Belize (BZ14RP) and Coral Gardens, Belize (CG14) to reconstruct seasonal cyclicity in coral geochemistry. Corals were sampled at 4, 6, 8, 10 samples per coral year for $\delta^{18}O$ and $\delta^{13}C$ to determine the best sampling resolution to represent maximum seasonality, which yielded an optimal resolution of 10 samples per year. From 4 to 10 samples per year, the Pleistocene coral BZRP12 expressed a larger $\delta^{18}O$ range by 1.81‰ and a larger $\delta^{13}C$ range by 1.56‰. For annually resolved data, $\delta^{18}O$ ranged 0.94‰ in the modern coral and 1.32‰ and 2.13‰ in the Pleistocene corals. $\delta^{13}C$ ranged 1.14‰ in the modern coral and 1.72‰ and 1.96‰ in the Pleistocene corals. We interpret the higher range in Pleistocene $\delta^{18}O$ and $\delta^{13}C$ to reflect a higher latitudinal range of the Intertropical Convergence Zone at that time. The $\delta^{18}O$ of our corals likely reflects precipitation and/or temperature, whereas $\delta^{13}C$ may reflect seasonal change in the flux of terrestrial 'light' carbon to the reef. Maximum seasonal paleotemperature change (if $\delta^{18}O$ reflects only temperature and no 'salinity' effect) calculated from $\delta^{18}O$ data suggest that the maximum seasonal range in temperature of the modern coral was the lowest (4.7°C), BZRP14 geochemistry represented a larger seasonal range (6.6°C), and BZRP12 expressed the largest seasonal range (10.7°C). These results support that increased summer insolation and decreased winter insolation acting on the Northern Hemisphere enhanced seasonality during the last interglacial.

## I. Introduction

While it has been established that the warmer climate of the last interglacial period was similar to that of today, the question remains as to whether the magnitude of the seasonal temperature cycle was enhanced relative to the modern (Felis et al., 2004; Winter et al., 2003). Although some studies have explored seasonal cycle amplitudes of the last interglacial, few (Al-Rousan et al., 2013; Felis et al., 2015; Winter et al., 2003) have discussed this topic in the context of the Caribbean, a tropical region heavily influenced by solar insolation. Previous research from multiple study localities has proposed that the last interglacial experienced a larger range in annual temperature and/or precipitation values during seasonal cycles (Felis et al., 2004; Suzuki et al., 2001; Winter et al., 2003). Some have shown evidence for an amplified interglacial seasonal cycle as reported from isotopic records of corals from the Red Sea, Bonaire (southern Caribbean), Isle de Mona (northeastern Caribbean), and the Pacific Ocean (Felis et al., 2004; Felis et al., 2015; Winter et al., 2003; Suzuki et al., 2001). In order to determine if the last interglacial experienced a larger seasonality and if this seasonality affected Caribbean climate, this study used sclerochronology and stable carbon ($\delta^{13}C$) and oxygen ($\delta^{18}O$) isotopic records as proxies for seasonal range in temperature and/or salinity and carbon cycle dynamics. We analyzed two modern and two Pleistocene *Orbicella sp.* corals (formerly *Montastrea sp.*) from Rocky Point, Belize and Coral Gardens, Belize as a proxy to compare seasonality at the last interglacial with that of today.

### *1. Pleistocene Climate*

The last interglacial period, synonymous with the Eemian on land and Marine Isotope Stage 5e, began ~130 Ka and terminated ~117 Ka (Kukla et al., 2002). This period was characterized by stronger orbital insolation forcing, warmer temperatures, and higher sea level (Felis et al., 2015). It is believed that the last interglacial period experienced stronger solar insolation during Northern Hemisphere summer than today, and a reduced solar insolation during Northern Hemisphere winter than today (Winter et al., 2003).

*2. Milankovitch Cycles*

Comparatively, the last interglacial and the modern are coincident with different Milankovitch parameters, which dictate global climate. Orbital forcing parameters can alter global insolation distribution, shifting positive or negative feedback cycles to drive climate into or out of a glacial or interglacial period (Maslin and Brierley, 2015). The strong Northern Hemisphere summer solar insolation and weakened Northern Hemisphere winter insolation during the last interglacial are consistent with specific parameters of Milankovitch cycling – eccentricity, obliquity, and precession (Winter et al., 2003). Eccentricity refers to the ellipticity of the earth's orbit around the sun, obliquity refers to the angle between the earth's rotational axis and its orbital axis, and precession refers to the change in the orientation of the rotational axis of the earth as it rotates (Ruddiman, 2001).

During the last interglacial period, Milankovitch calculations yield a suggested 10.54% increase in summer insolation at 18˚N and a 9.69% decrease in winter insolation at 18˚N (Winter et al., 2003) (Fig. 1). This is a result of the earth's more elliptical orbit, minimum precession, and greater obliquity at that time (Winter et al., 2003). Eccentricity dictates the timing of perihelion (the point at which the earth is closest to the sun during its orbit), with perihelion during Northern summer enhancing seasonality and perihelion during Northern winter enhancing seasonality to a lesser extent (Merlis et al., 2012). Between 128 Ka and 124 Ka, perihelion occurred during Northern Hemisphere summer instead of Northern Hemisphere winter, which strengthened the seasonality of insolation (Kim, 2010; Winter et al., 2003). Currently, the opposite exists, which effectively dampens the amplitude of temperature and precipitation cycles (Winter et al., 2003; Kim, 2010). A greater axial tilt creates more dramatic seasons, which would augment the contrast between hemispheres during summer and winter (Winter et al., 2003). Minimum precession enhances Northern Hemisphere seasonality and dampens Southern Hemisphere seasonality (Winter et al., 2003). It is not the amount of solar insolation received by the earth, but the seasonal and latitudinal variation of this insolation that forces climate (Ruddiman, 2006).

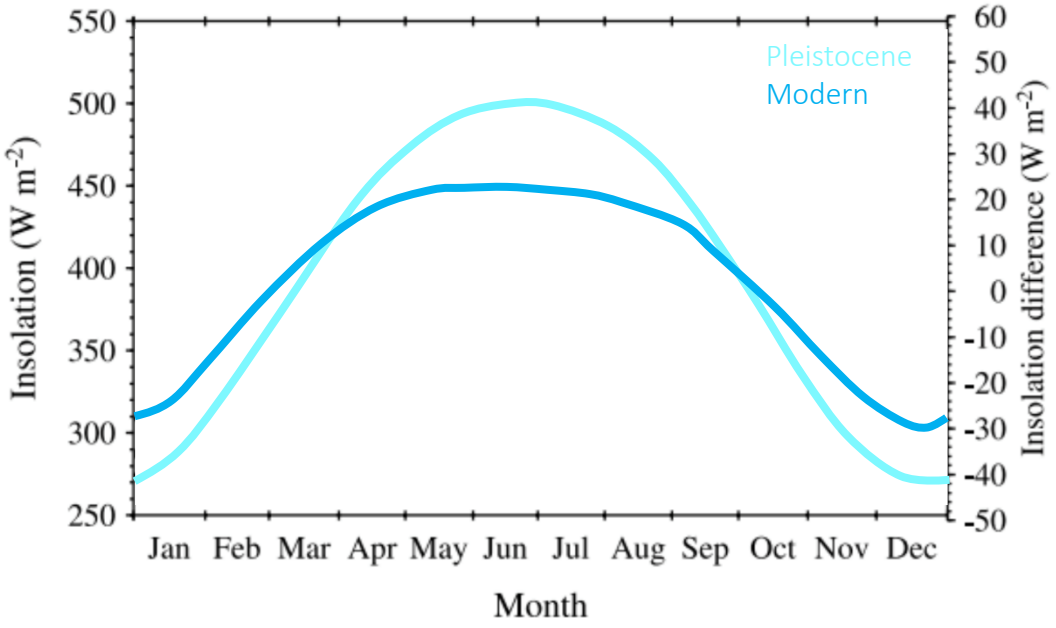


**Fig. 1:** Insolation variability at 18°N during the Pleistocene and during the modern for one annual cycle. During Northern Hemisphere summer, Pleistocene local insolation was 10.54% higher than today but 9.69% lower than today during Northern Hemisphere winter (Winter et al., 2003).

*3. Intertropical Convergence Zone*

This seasonal and latitudinal variation of solar insolation may have resulted in a more northward and latitudinally extensive Intertropical Convergence Zone (ITCZ, the climatic equator) over the Caribbean during the Pleistocene. The position of maximum solar insolation dictates the region on earth that is the hottest, causing air to rise quickly, creating a low-pressure zone at the convergence between north-easterly and south-easterly trade winds (Linsley et al., 1994; Schneider et al., 2015). The ITCZ is characterized by strong convection and heavy precipitation, primarily above the ocean (Linsley et al., 1994; Schneider et al., 2015). It migrates latitudinally over geologic time, on a seasonal scale and longer (Schneider et al., 2015). Annual fluctuation of the ITCZ controls seasonal variability at tropical latitudes (Linsley et al., 1994). During periods of high seasonality, the ITCZ reaches a larger spatial extent, meaning that it introduces an influx of precipitation into the Belizean reef system during part of the year, but is absent

during the rest of the year, creating more arid conditions at the study locality. During periods of attenuated seasonality, the ITCZ isn't as mobile, meaning that Belize is covered by the ITCZ during the majority of the year, so precipitation is more constant. Due to the strengthened Northern Hemisphere seasonality during the last interglacial, the spatial variation of the ITCZ would presumably have led to higher amplitude seasonal temperature and/or precipitation cycles at that time.

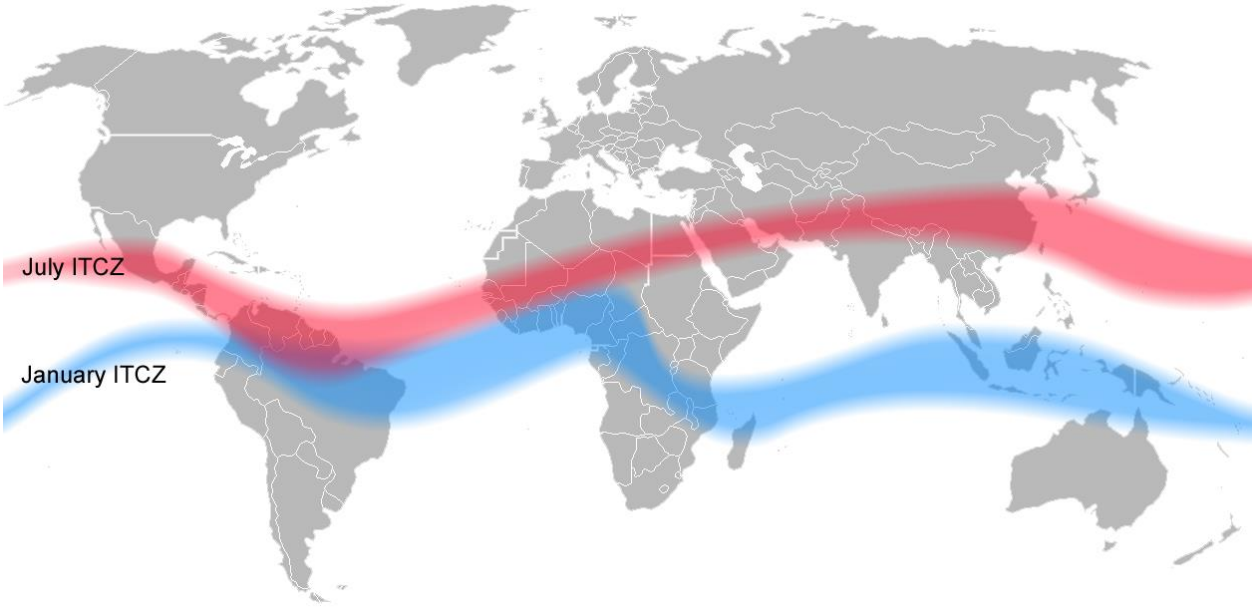


**Fig. 2:** Spatial variation of the ITCZ on a seasonal time scale (Wikipedia, 2016).

*4. Coral Sclerochronology*

Coral sclerochronology is a useful tool for reconstructing annually resolved climate trends (Leder et al., 1996). Scleractinian corals grow in shallow waters, and thus reflect sea surface conditions (Corrège, 2006). They grow linearly, as the coral polyp secretes aragonite (Corrège, 2006). The rate of growth (linear extension rate) is highly dependent upon photosynthesis rates (Druffel, 1997). Since linear extension rate (LER) is modulated by photosynthesis, corals grow alternating bands of dense and less dense aragonite, depending on the season (Swart, 1982). A coupled high and low density band represents an annual cycle of growth where density variations represent changes in the rate of skeletal LER and calcification (Leder et al., 1996; Druffel, 1997; Al-Rousan et al., 2013). LER represents unidirectional, linear growth of the

coral and calcification represents total skeletal mass accumulation per area per time (Corrège, 2006). Linear extension has an inverse relationship with density and positive relationship with calcification (Druffel, 1997). This study sampled along the principle growth axis where LERs are maximized and isotopic disequilibria is most constant (Leder et al., 1996).

*5. Stable Isotopes*

The geochemistry of corals are useful for paleoclimate interpretation because they form in isotopic disequilibria with surrounding seawater (McConnaughey, 1989). During aragonite accretion, oxygen and carbon isotopes fractionate due to thermodynamics and coral physiology (McConnaughey, 1989). Both carbon ($^{13}C/^{12}C$ ratio) and oxygen ($^{18}O/^{16}O$ ratio) isotopic compositions incorporated during aragonite accretion are influenced by environmental parameters (Al-Rousan et al., 2013). Corals are usually depleted in $\delta^{13}C$ and $\delta^{18}O$ relative to ambient seawater, which occurs from either kinetic effects or metabolic effects (Swart, 1983; McConnaughey, 1989). The delta notation refers to the relative enrichment or depletion of the heavier isotope in the coral sample relative to a standard (McConnaughey, 1989).

*5.1 Carbon Isotopes*

Skeletal $\delta^{13}C$ composition is a function of the $\delta^{13}C$ of DIC in seawater and how it fractionates through photosynthesis and respiration (McConnaughey, 1989). Whereas photosynthesis increases $\delta^{13}C$, respiration decreases $\delta^{13}C$ (McConnaughey, 1989). However, in corals, photosynthesis plays a more important role than respiration in skeletal isotopic composition (McConnaughey, 1989). Due to the fact that the majority of skeletal carbon originates from dissolved inorganic carbon (DIC) in seawater, coral $\delta^{13}C$ reflects the carbon isotopic composition of sea water present during coral growth, which in turn reflects the environmental parameters at that time (Druffel, 1997). Coral polyps obtain DIC from seawater through metabolic processes such as photosynthesis and heterotrophy (Grottoli, 2000). Symbiotic algae called zooxanthellae live in coral tissue and generate isotopic fractionation by providing the coral with fixed carbon from seawater (Grottoli, 2000). Zooxanthellae preferentially consume $^{12}C$ during

photosynthesis, leaving $^{13}C$ for aragonite accretion (Al-Rousan et al., 2013). Increased exposure to sunlight during warmer seasons facilitates increased photosynthesis by symbiotic algae, leading to a higher $\delta^{13}C$ (McConnaughey, 1989; Swart, 1983; Al-Rousan et al., 2013).

*5.2 Oxygen Isotopes*

The $\delta^{18}O$ signature recorded in scleractinian corals is commonly used as a proxy for paleotemperature (Corrège, 2006; Grottoli and Eakin, 2007). Coral $\delta^{18}O$ is most often governed by sea surface temperature and/or the 'isotopic effect' which co-varies with salinity (Leder et al., 1996; Swart et al., 1983; Druffel, 1997). Theoretically, if salinity is presumed relatively constant throughout time, $\delta^{18}O$ can be used as an indicator of paleotemperature range, where the relationship between $\delta^{18}O$ and sea surface temperature has been determined to change 1°C for every 0.22 per mil deviation for the species Orbicella (formerly Montastraea) (Leder et al., 1996; Druffel, 1997). Preferential uptake of $^{18}O$ into skeletal aragonite during colder periods and preferential uptake of $^{16}O$ during warmer periods results from temperature dependent fractionation (Kim and O'Niel, 1997). If seawater is $\delta^{18}O$ deficient, so is the coral skeleton (Grottoli and Eakin, 2007). $\delta^{18}O$ deficiency in seawater results from increased precipitation or from changes in the isotopic composition of the water entering the system (Grottoli and Eakin, 2007). Precipitation in the tropics is depleted in $^{18}O$ relative to seawater and evaporation preferentially removes $^{16}O$ from the ocean, leaving behind $^{18}O$ (Gagan et al., 2000). Thus, increased rainfall during wet months can decrease $\delta^{18}O$ and salinity of seawater (Linsley et al., 1994; Grottoli and Eakin, 2007).

As previously stated, this study aims to determine (1) whether the geochemistry of our corals expresses different magnitudes of temperature and/or precipitations cycles and (2) the optimal sampling resolution for most effectively capturing the seasonal cycle of a coral year. The increased summer insolation but decreased winter insolation acting on the Northern Hemisphere during the last interglacial should be reflected by the isotopic records of our corals, via $\delta^{13}C$ (light) and $\delta^{18}O$ (temperature and/or

precipitation). By comparing the geochemistry of the modern corals with the Pleistocene corals, we expect to see the effect of orbital forcing on seasonality of Caribbean climate.

## II. Study Locality

Three individual coral samples were taken from Rocky Point, Belize (N 18°10'32", W 087°50'11"). Two Pleistocene corals, hereafter referred to as BZRP12 and BZRP14, were acquired from a fossil reef in 2002. One modern coral core, hereafter referred to as BZ14RP, was obtained from Rocky Point in 2014. Another modern coral, hereafter referred to as CG14, was retrieved from Coral Gardens, Belize in 2014.

Belize experiences the general climate conditions of the Caribbean. As shown in Figure 3, Rocky Point is located at the northern tip of Ambergis Caye and is characterized by a rocky, sandy shoreline (DeCorte, 2015). Just beyond Rocky Point, the Mesoamerican barrier reef merges with the land (Greer, personal communication). Due to the close proximity of the land and the barrier reef, the lagoon is small and not well developed, but the Rocky Point modern reef is protected from reef break (Greer, personal communication). The Rocky Point patch reefs today grow in very shallow (~2m water depth) water. The Pleistocene terrace at Rocky Point, where BZRP12 and BZRP14 were collected, represents a shallow water fringing reef that deepens seaward (Greer, personal communication).

Coral Gardens, located to the south of Rocky Point, is a system of patch reefs in a back reef lagoonal setting of 4-8m water depth (Busch et al., 2015). It is located inland of the Mesoamerican barrier reef, and experiences more open marine circulation than Rocky Point (Greer, personal communication).

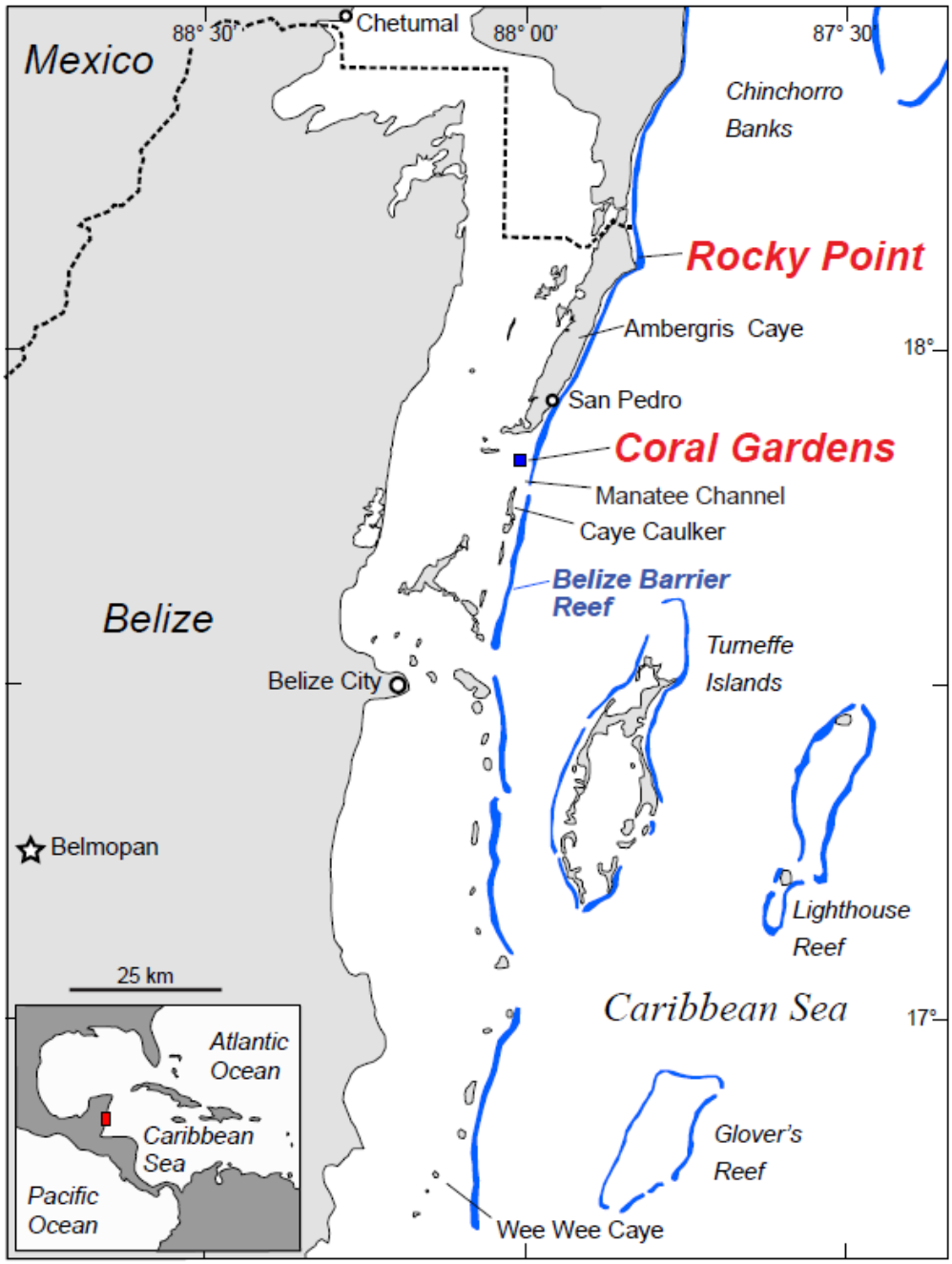


**Fig. 3:** Map of coastal Belize, showing the sampling localities of Rocky Point and Coral Gardens. Blue areas represent active reefs (DeCorte 2015).

## III. Methodology

Two Pleistocene aged corals (BZRP12 and BZRP14) were collected in 2002 by Lisa Greer and Jill Leonard-Pingel from a fossil reef at Rocky Point, Belize. The corals were sliced into slabs of 3 mm thickness along the axis of upward corallite growth and attached to glass slides (Fig. 4A). Data generated from the Pleistocene coral by the following methodology were compared with the modern corals, which were processed and sampled similarly by DeCorte, 2015.

X-radiographs were obtained for four coral slabs by using a Progeny Preva digital x-radiography machine at the Shenandoah Dental Studio in Lexington, VA. Each composite coral x-radiograph, shown here in Fig. 4B, was a compilation of six individual images that were assembled using Adobe Photoshop. Metal staples were placed on the coral surface to orient the sample's vertical growth direction.

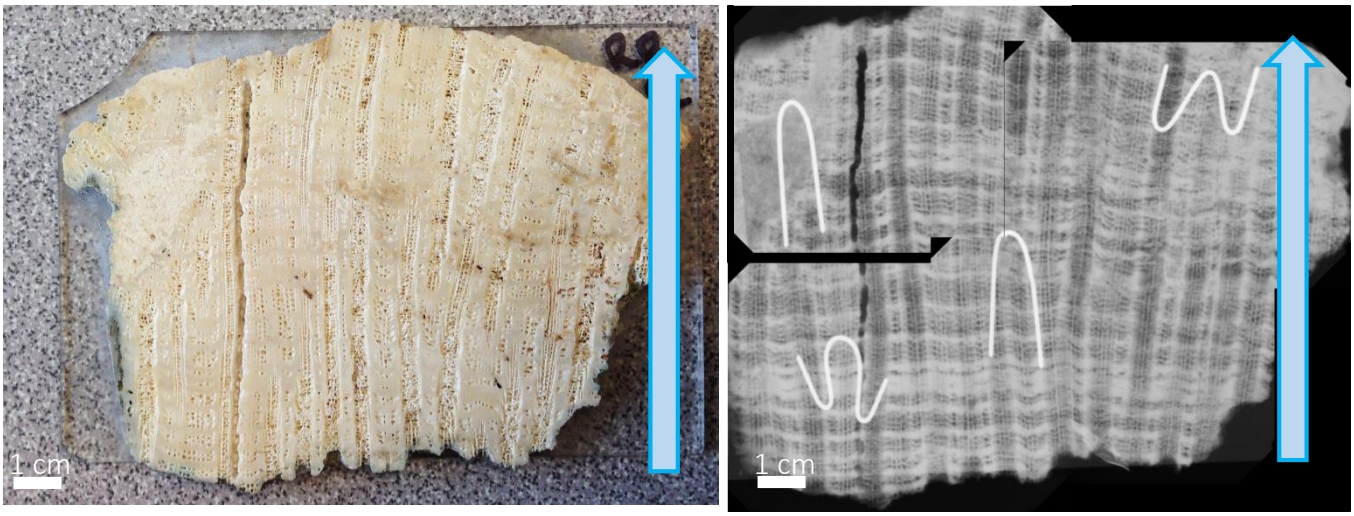


**Fig. 4A:** Pleistocene coral slab BZRP12, with relic drilling transect on the left. Arrow denotes direction of growth.

**Fig 4B:** X-radiograph of Pleistocene coral BZRP12, with relic drilling transect on the left. White lines represent metal staples used to orient the photos for the composite image. Arrow denotes direction of growth.

Corals were sonicated and washed in a 10% Hydrogen Peroxide solution before drilling. A 500mL beaker was thoroughly rinsed with deionized water and then refilled with deionized water. This beaker was placed in the water-filled TransSonic TS 400 basin. Each sample was sonicated three times, for five minutes

each time. Between each sonication, the beaker containing the sample was drained and refilled with deionized water.

Linear Extension Rates (LER) were calculated using ImageJ and verified by measuring the distance between density peaks on an x-radiograph photocopy using a ruler. Using the methodology developed by DeCorte, 2015, coral x-radiographs were imported into ImageJ to create digital number profiles (DNP), which are quantifications of grayscale variations along a given transect (DeCorte, 2015). The digital number profile data was scaled to the coral's physical measurements. Peaks of the highest DNP values were identified and distances between adjacent peaks were considered to be one coral growth year. The lightest bands on the x-radiograph represent the densest aragonite bands on the coral and the darkest areas on the x-radiograph represent the least dense aragonite bands. This process was repeated for multiple transects for a given coral sample, after which all mean growth rates were averaged together as a set to determine the mean LER of the coral. To corroborate these calculations, the same transects that were analyzed in ImageJ were measured with a ruler. The individual measurements of each coral year were averaged and the standard deviation was calculated. The mean growth rate of each transect was averaged together as a set to determine the mean LER of the coral.

The x-radiographs of each coral sample were printed at the same scale as the actual coral slab. Translucent paper was overlain onto the x-radiograph and the coral years were traced onto the paper, which was then overlain onto the coral sample and placed on the MicroMill stage. BZRP12, BZRP14, and BZ14RP were microsampled along thecal walls using a Merchantek MicroMill. Using MicroMill System Version 1.4.1.0, horizontal drilling lines were marked parallel to growth bands, within one thecal wall. One line was drawn at the start of one growth band and then copied nine times along the axis of vertical growth to the end of the year, still within the same thecal wall. This standardized the angle and distance between drill lines.

Both the Pleistocene and modern corals were sampled in two different ways to satisfy two different objectives. Initially, we wanted to determine the optimal sampling resolution per coral year in order to most effectively capture the seasonal cycle in one coral growth year. For a laterally continuous period of two coral years, samples were taken from four different thecal walls at four different resolutions of 4, 6, 8 and 10 samples per year (Fig. 5).

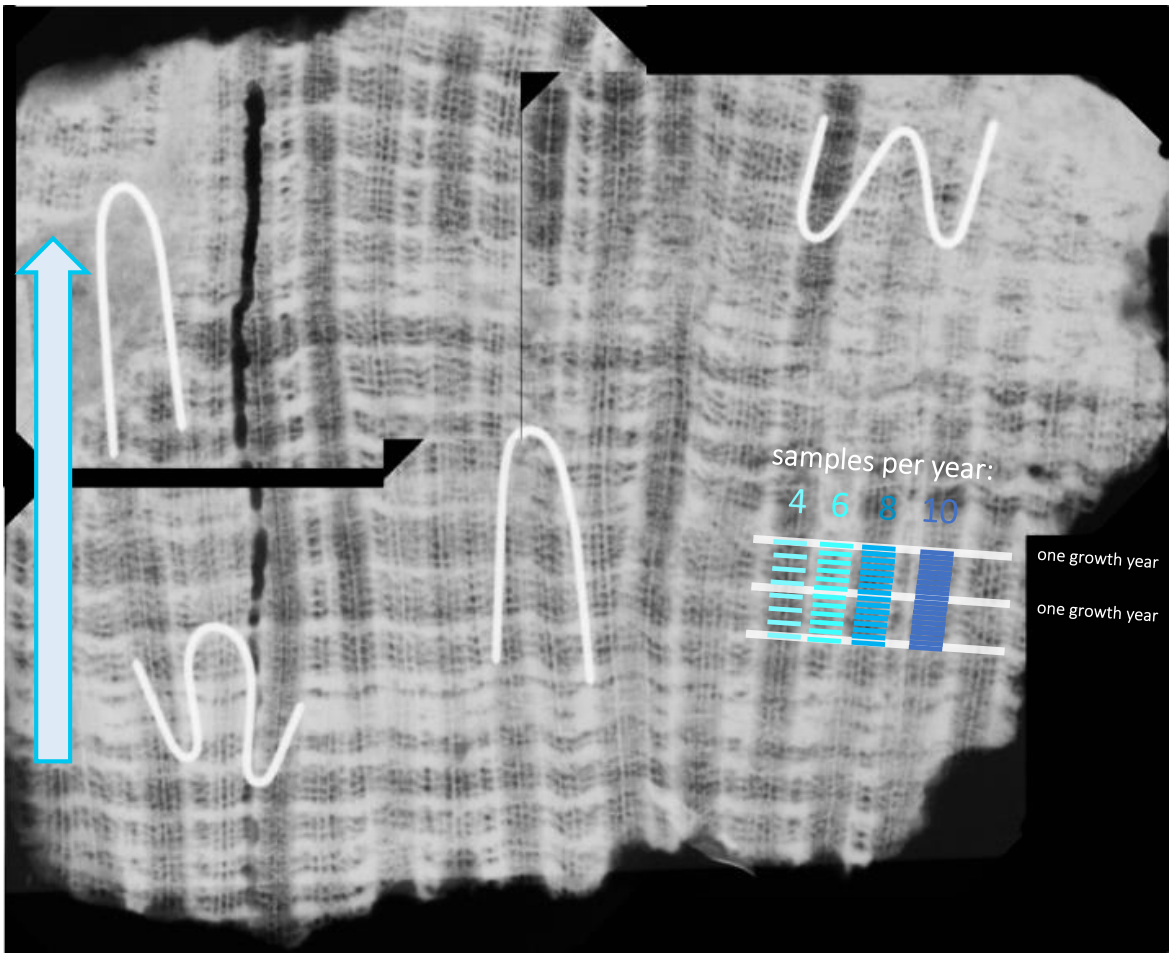


**Fig. 5:** X-radiograph of Pleistocene coral BZRP12, annotated with sampling resolution methodology.

The second task was to produce a high resolution, decadal long isotopic record from both corals. Most coral years were drilled at a resolution of 10 samples per year, with a few exceptions of 8 samples per year for particularly dense years. After a line was drilled, the coral was removed from the stage, the aragonite powder was tapped into labeled weighing paper and then stored in a labeled vial. The sample

and drill bit were cleaned with compressed air between generation of each sample powder. This process was repeated for 310 samples.

Aragonite powder obtained from drilling was analyzed using Washington and Lee University's Thermo-Scientific Stable Isotope Ratio Mass Spectrometer. All vials were held in the GC Pal Autosampler at 21 ℃ during analysis. However, samples were flushed by two different methods. For the first method, the samples were flushed for ten minutes each with the Finnigan GasBench II by replacing the atmospheric air in the vial with 99.9999% helium. After the samples had been flushed, 0.02 mL of Sigma-Aldrich 99.0% pure $H_3PO_4$ were added into each pressurized vial directly onto the sample powder using a needle and syringe. For the second flushing method, the sample vials were placed horizontally in a tray. Still in the horizontal orientation, with the powder at the very bottom of the vial, 0.02 mL of the $H_3PO_4$ were added at the top of the vial to prevent interaction of the sample and acid. Ten samples at a time were horizontally attached to a flushing manifold that was coupled with the helium tank. After flushing for ten minutes, each vial was returned to a vertical position, which facilitated the interaction of the acid with the powder. Each powdered sample reacted with the acid for at least one hour to produce $CO_2$ gas.

Before the samples could be analyzed, we ran a Zero Enrichment Test, which is an overall performance test that runs 10 sets of 10 99.995% $CO_2$ peaks to ensure that the machine is functioning properly (GasBench II Operating Manual, Thermo Fisher Scientific). We only report data that reached a $\delta^{13}C$ external error of less than 0.06, which signifies the standard deviation of the mean values of all measurements (GasBench II Operating Manual, Thermo Fisher Scientific). After satisfying this threshold, our samples were analyzed on the mass spectrometer via the gasbench. Three standards (NBS-19, limestone) were flushed and two were added to the beginning of each sequence and one to the end of each sequence for standard calibration. $\delta^{18}O$ and $\delta^{13}C$ ratios are reported as per mil (‰) deviations relative to SMOW and VPDB, respectively. This calculation is outlined by the equation stated by McConaughey, 1989, where $R_{sample}$ represents the raw $^{13}C/^{12}C$ and $^{18}O/^{16}O$ of the sample, $R_{SMOW}$ and $R_{PDB}$ represent the

$^{13}C/^{12}C$ and $^{18}O/^{16}O$ global standards derived from Standard Mean Ocean Water and the Vienna Pee Dee belemnite (Equation 1).

$$\delta^{18}O \text{ or } \delta^{13}C = \frac{R_{sample} - R_{standard}}{R_{standard}} * 1000 \quad (1)$$

In order to separate the glue bonding between the Pleistocene coral slabs and the glass slides, they were submerged overnight in GooGone. An industrial razor was then used to decouple the coral slabs from the glass slides. Roughly 5g of sample was removed from BZRP12 after it had been sonicated by the aforementioned procedure, following the methodology created by Clark et al., 2014. A mortar and pestle, which were cleaned with DI water, were used to crush the sample into ~2mm sized pieces. These granules soaked overnight in a 10% hydrogen peroxide, Milli-Q dilution. In the morning, they were rinsed with Milli-Q water and centrifuged with the hydrogen peroxide solution for 15 minutes at 4,000 rpm. They were again sonicated in Milli-Q water. Once dry, the fragments were examined under a binocular microscope to remove any impurities that may have altered the $^{230}Th/^{234}U$ results. This sample was sent to the Radiogenic Isotope Facility at the University of Queensland for $^{230}Th/^{234}U$ dating.

## IV. Results

### *1. Linear Extension Rates*

LER data obtained from our corals was plotted to compare the trends between the two Pleistocene corals (BZRP12, BZRP14) and the modern coral (BZ14RP) (Fig. 6). The mean LER for the modern coral BZ14RP was 10.35±1.56 (n=31), the mean LER for the Pleistocene coral BZRP12 was 2.48±0.95 (n=71), and the mean LER for the Pleistocene coral BZRP14 was 2.84±0.66 (n=47) (Table 1). We also calculated the mean LER of BZRP14 by hand to compare it with the LER given by the ImageJ method and obtained a mean LER of 2.83±0.68 (n=47).

| | **Mean LER (mm)** | **Stdev** |
|---|---|---|
| **Pleistocene (BZRP12)** | 2.48 | 0.95 |
| **Pleistocene (BZRP14)** | 2.84 | 0.66 |
| **Modern (BZ14RP)** | 10.35 | 1.56 |

**Table 1:** LER data obtained from the methodology developed by DeCorte 2015.

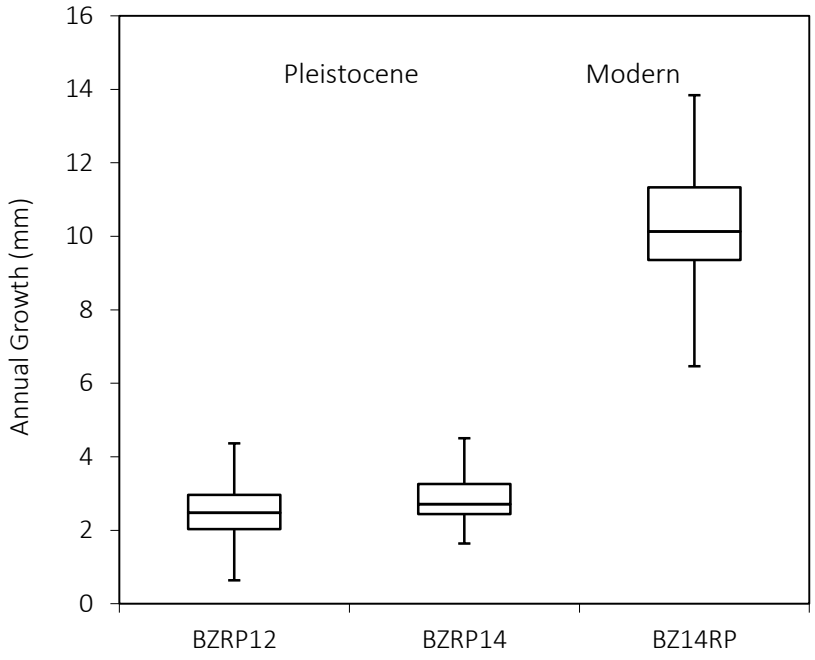


**Fig. 6:** Box Plot representation of LER data obtained from the methodology developed by DeCorte 2015.

*2. External Calibration*

In order to verify the accuracy of Washington and Lee's new stable isotope ratio mass spectrometer, 20 sample splits were sent to Dr. Peter Swart at the Rosenstiel School of Marine and Atmospheric Science at the University of Miami (Fig. 12 & 15). The average difference between $\delta^{13}C$ values was 0.24‰ whereas the average difference between $\delta^{18}O$ values was -0.03‰. T-test analysis confirms that the difference between the sample splits were statistically insignificant (p=0.61, p=0.16, respectively). The small deviation between the sample splits validates the authenticity of our data.

*3. Sampling Resolution*

*3.1 Oxygen*

Table 2, along with Figures 7A & 7B, shows $\delta^{18}O$ sampling resolution data from the Pleistocene coral BZRP12 and the modern coral BZ14RP. At the lowest sampling resolution (4 samples per year), the mean $\delta^{18}O$ values for the Pleistocene and modern coral were similar at -4.19‰ and -3.96‰ respectively. The Pleistocene coral (BZRP12) had a larger seasonal $\delta^{18}O$ range of 0.66‰ compared to the modern coral (BZRP14) range of 0.40‰. At the highest sampling resolution (10 samples per year), the mean $\delta^{18}O$ values for the Pleistocene and modern coral were similar at -3.64‰ and -3.95‰ respectively. The Pleistocene and modern $\delta^{18}O$ indicated seasonal ranges of 2.47‰ and 0.99‰, with the Pleistocene seasonal $\delta^{18}O$ range exceeding that of the modern coral by 1.48‰. The $\delta^{18}O$ range indicated by the Pleistocene coral at the highest sampling resolution was 1.81‰ larger than the $\delta^{18}O$ range indicated by the Pleistocene coral at the lowest sampling resolution.

| | | **$\delta^{18}O$ mean** | **$\delta^{18}O$ range** | **$\delta^{13}C$ mean** | **$\delta^{13}C$ range** |
|---|---|---|---|---|---|
| 4 samples/year | **Pleistocene (BZRP12)** | -4.19 | 0.66 | -1.08 | 1.75 |
| | **Modern (BZR14RP)** | -3.96 | 0.41 | -0.92 | 1.83 |
| 10 samples/year | **Pleistocene (BZRP12)** | -3.64 | 2.47 | -1.34 | 3.31 |
| | **Modern (BZR14RP)** | -3.95 | 0.99 | -0.97 | 1.83 |

**Table 2:** Isotopic means and seasonal ranges of both the Pleistocene and modern corals at two different sampling resolutions, 4 samples per year and 10 samples per year.

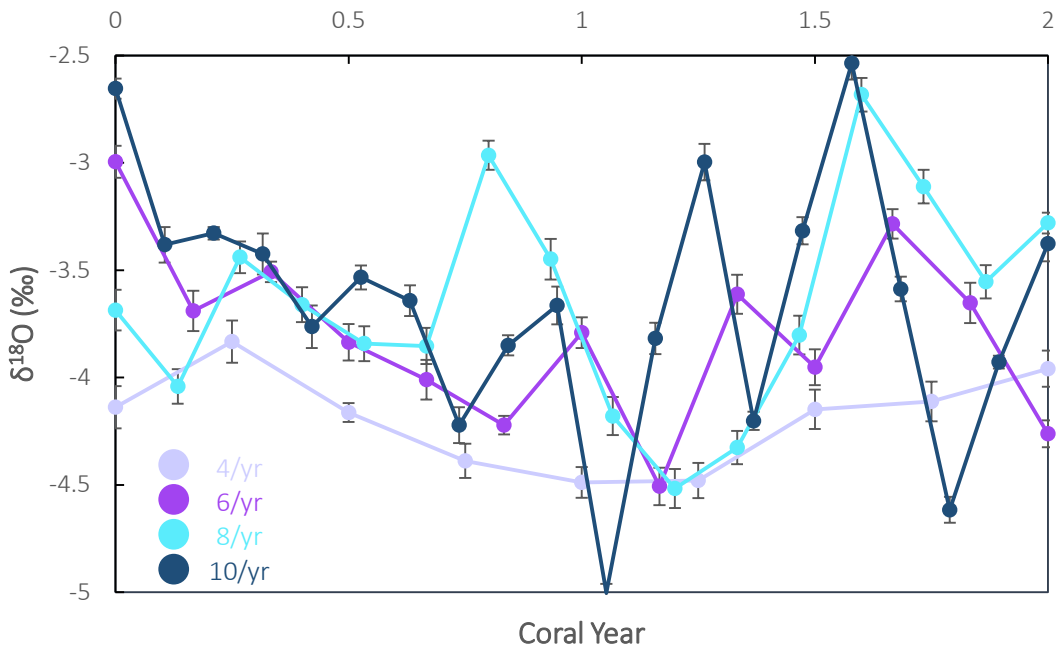


**Fig. 7A:** $\delta^{18}O$ sampling resolution data from the Pleistocene coral BZRP12.

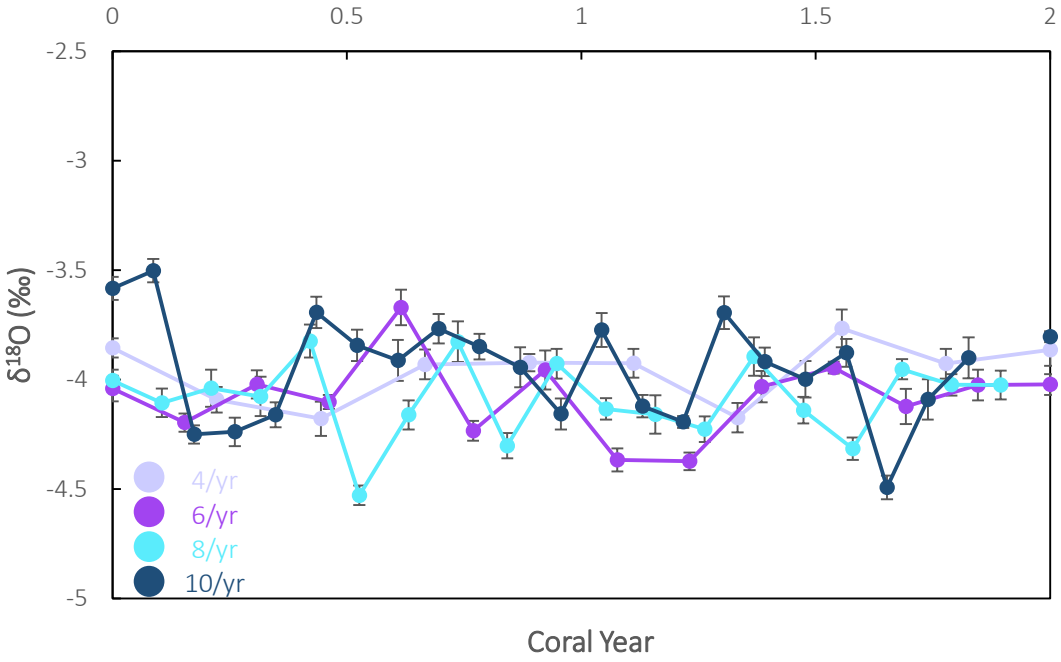


**Fig. 7B:** $\delta^{18}O$ sampling resolution data from the modern coral BZ14RP.

*3.2 Carbon*

Table 2, along with Figures 8A & 8B, shows $\delta^{13}C$ sampling resolution data from the Pleistocene coral BZRP12 and the modern coral BZ14RP. At the lowest sampling resolution (4 samples per year), the mean $\delta^{13}C$ values for the Pleistocene and modern coral were -1.08‰ and -0.92‰ respectively, but the Pleistocene coral had a seasonal $\delta^{13}C$ range of 1.76‰ compared to the modern coral range of 1.83‰. At the highest sampling resolution (10 samples per year), the mean $\delta^{13}C$ values for the Pleistocene and modern coral were -1.34‰ and -0.97‰ respectively. The Pleistocene and modern $\delta^{13}C$ indicated seasonal ranges of 3.31‰ and 1.83‰. At the highest sampling resolution, the Pleistocene seasonal $\delta^{13}C$ range was greater than that of the modern coral by 1.49‰. The $\delta^{13}C$ range indicated by the Pleistocene coral at the highest sampling resolution was 1.56‰ larger than the $\delta^{13}C$ range indicated by the Pleistocene coral at the lowest sampling resolution.

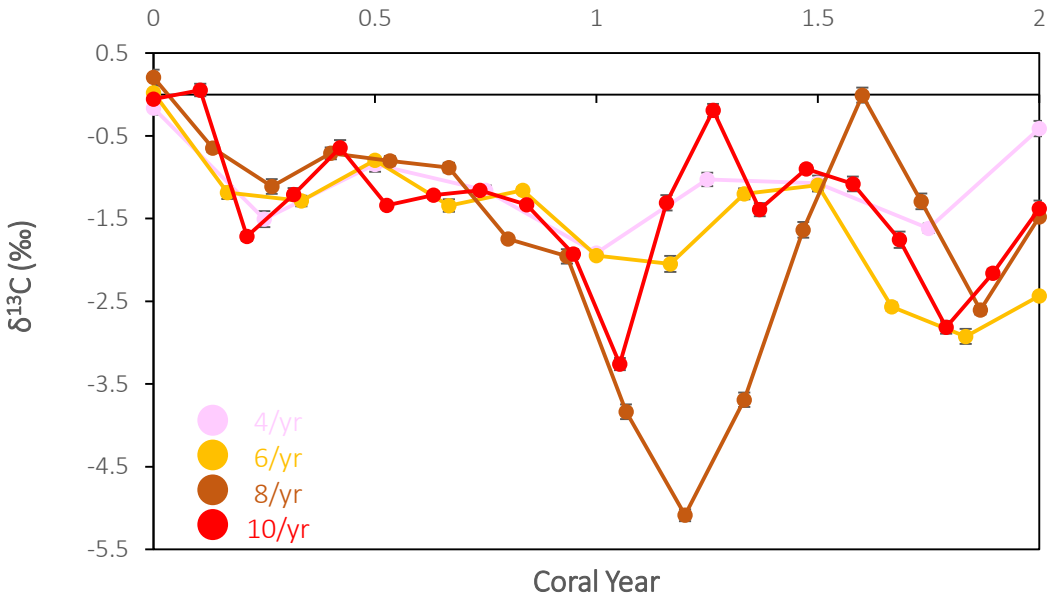


**Fig. 8A:** $\delta^{13}C$ sampling resolution data from the modern coral BZRP12.

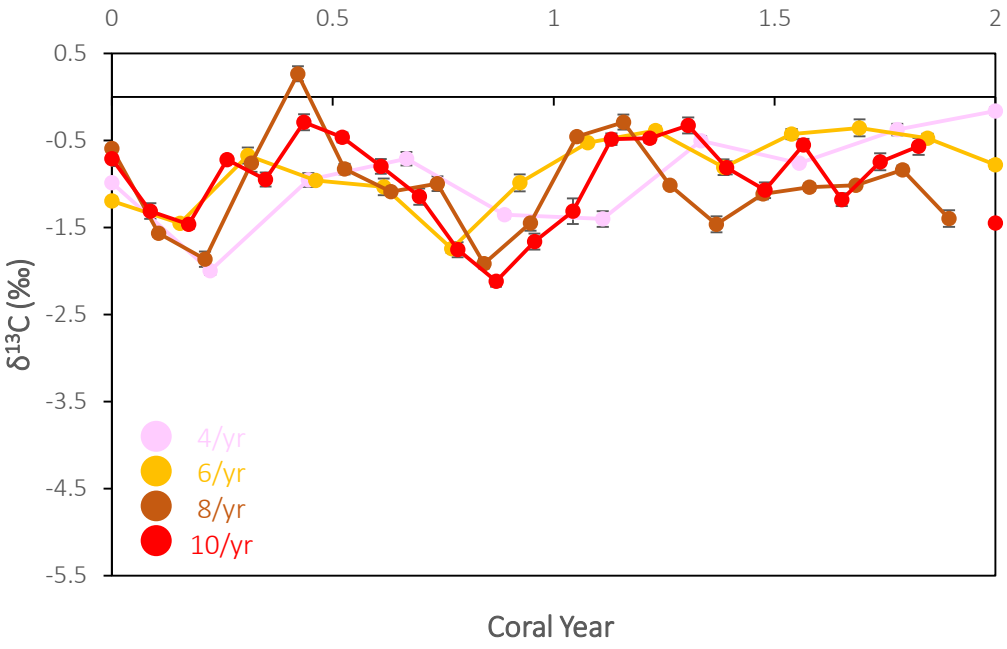


**Fig. 8B:** $\delta^{13}C$ sampling resolution data from the modern coral BZ14RP.

*4. Stable Isotope Transects*

*4.1 Bulk Isotopic Signatures*

Table 3, along with Figures 9A & 9B, represents the bulk data population for the entire transect drilled per coral sample. Of the two Pleistocene corals, the bulk mean $\delta^{18}O$ was lighter for BZRP12 (-4.42‰ ± 0.86; n=124) than that of BZRP14 (-3.74‰ ± 0.58 n=62). The bulk mean $\delta^{13}C$ was also lighter for BZRP12 (-1.20‰ ± 0.74; n=124) than BZRP14 (-0.29‰ ± 0.62 n=62). However, the bulk mean $\delta^{13}C$ for the modern coral BZ14RP (-0.62‰ ± 0.55; n=23) was isotopically heavier than one Pleistocene coral BZRP12 but lighter than the other Pleistocene coral BZRP14. The bulk mean $\delta^{18}O$ for the modern coral BZ14RP (-3.45‰ ± 0.40; n=23) was isotopically heavier than both Pleistocene corals BZRP12 and BZRP14.

| | **$\delta^{18}O$ mean** | **$\delta^{18}O$ stdev** | **$\delta^{13}C$ mean** | **$\delta^{13}C$ stdev** |
|---|---|---|---|---|
| **Pleistocene (BZRP12)** | -4.42 | 0.86 | -1.21 | 0.74 |
| **Pleistocene (BZRP14)** | -3.74 | 0.58 | -0.29 | 0.62 |
| **Modern (BZ14RP)** | -3.45 | 0.40 | -0.62 | 0.55 |
| **Modern (Coral Gardens)** | -4.19 | 0.89 | -0.90 | 0.82 |

**Table 3:** Bulk population isotopic means and variability of all four coral samples.

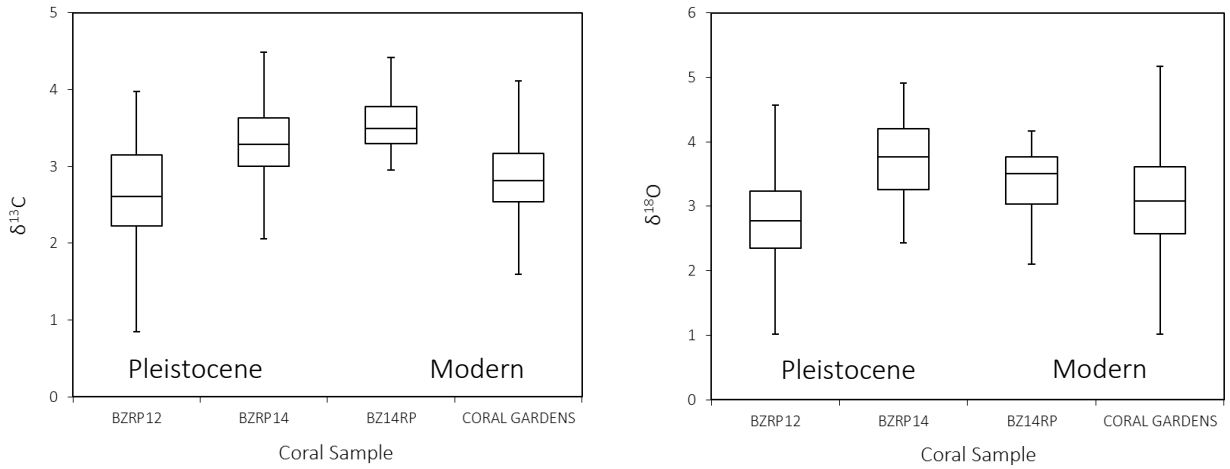


**Fig. 9A & 9B:** $\delta^{13}C$ and $\delta^{18}O$ bulk population data for both corals from the Pleistocene and both corals from the modern.

*4.2 Seasonal Ranges*

To annually resolve the entire dataset, each transect was segregated into coral years, based on interpretation of isotopic peak to peak or trough to trough. The seasonal range was calculated for each coral year by subtracting the minimum isotopic value within the coral year from the maximum isotopic value within the same coral year. After seasonal ranges were calculated for each year, all of these ranges were averaged together to find the mean seasonal range for the entire coral. Table 4 represents seasonal ranges calculated from annually averaged data.

Since $\delta^{18}O$ did not show as clear of a cyclical pattern as did $\delta^{13}C$, $\delta^{18}O$ annual populations were established in two different ways. $\delta^{18}O$ and $\delta^{13}C$ cycles are out of phase with respect to the linear extension of the coral – $\delta^{18}O$ cycles lag behind $\delta^{13}C$ cycles, so we interpreted the $\delta^{18}O$ cycles in two ways, either dependent or independent of where $\delta^{13}C$ cycles occurred along the coral's linear extension. The first set of $\delta^{18}O$ values in Table 4 represent ranges from coral years that were determined by interpretation of $\delta^{18}O$ isotopic peak to peak or trough to trough, independent of $\delta^{13}C$ defined coral years. The second set of $\delta^{18}O$ values in Table 4 represent ranges that correspond to coral years interpreted from $\delta^{13}C$ isotopic peaks/troughs.

| | $\delta^{18}O$ mean* | $\delta^{18}O$ stdev* | $\delta^{18}O$ mean | $\delta^{18}O$ stdev | $\delta^{13}C$ mean | $\delta^{13}C$ stdev |
|---|---|---|---|---|---|---|
| **Pleistocene (BZRP12)** | 2.11 | 1.20 | 2.13 | 1.41 | 1.96 | 0.77 |
| **Pleistocene (BZRP14)** | 1.73 | 1.52 | 1.32 | 1.20 | 1.72 | 0.31 |
| **Modern (BZ14RP)** | | | 0.94 | 0.39 | 1.14 | 0.69 |

* Independent years, not correlated with $\delta^{13}C$

**Table 4:** Mean seasonal ranges and seasonal range variability determined from annual populations.

The mean seasonal range of $\delta^{13}C$ was roughly the same for both Pleistocene corals BZRP14 and BZRP12 (1.71‰ ± 0.31; n=62 and 1.96‰ ± 0.77; n=124), whereas the standard deviation was much higher for BZRP12 by 0.46‰. For the Pleistocene coral BZRP12, $\delta^{18}O$ exhibited roughly the same seasonal range mean for independently defined years as well as $\delta^{13}C$-correlated years (2.11‰ ± 1.20; n=124 and 2.12‰ ± 1.41; n=124 respectively). For the other Pleistocene coral BZRP14, $\delta^{18}O$ with independently defined years exhibited a slightly higher seasonal range mean than $\delta^{13}C$-correlated years (1.73‰ ± 1.52; n=62 and 1.32‰ ± 1.20; n=62 respectively). The mean $\delta^{13}C$ seasonal range for the modern coral BZ14RP was (1.42‰ ± 0.69; n=23) and the mean $\delta^{18}O$ seasonal range was (0.94‰ ± 0.39; n=23).

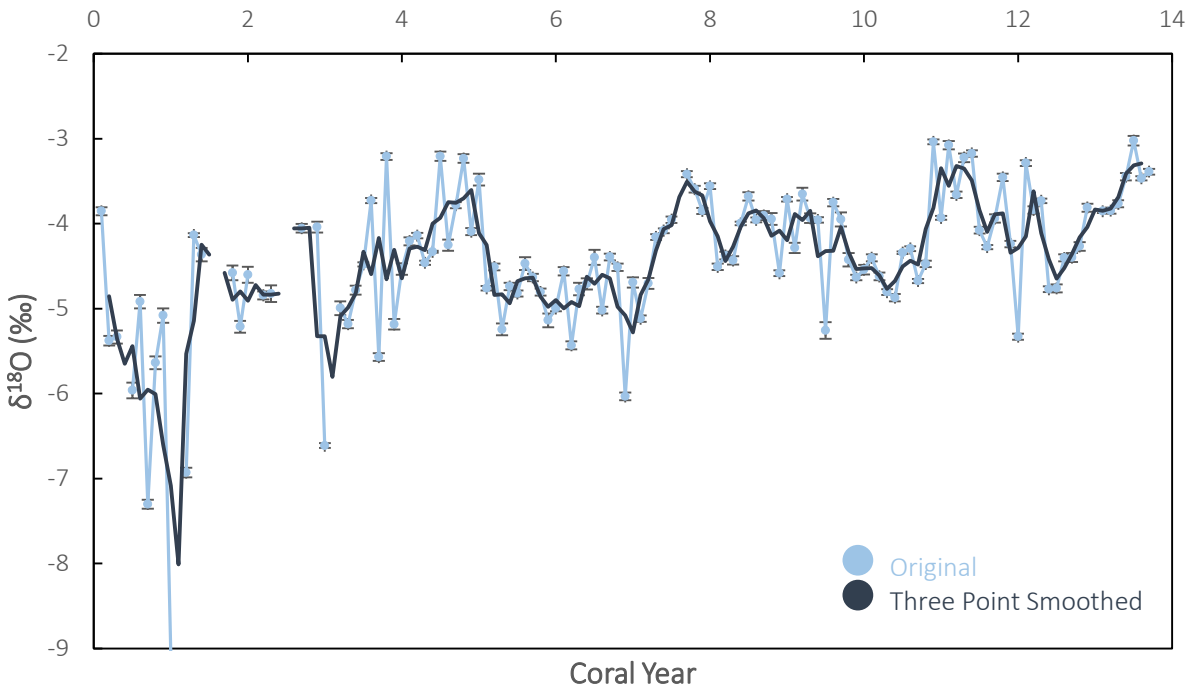


**Fig. 10:** $\delta^{18}O$ transect analysis of the Pleistocene coral BZRP12. A three-point smoothing analysis is superimposed on the raw data.

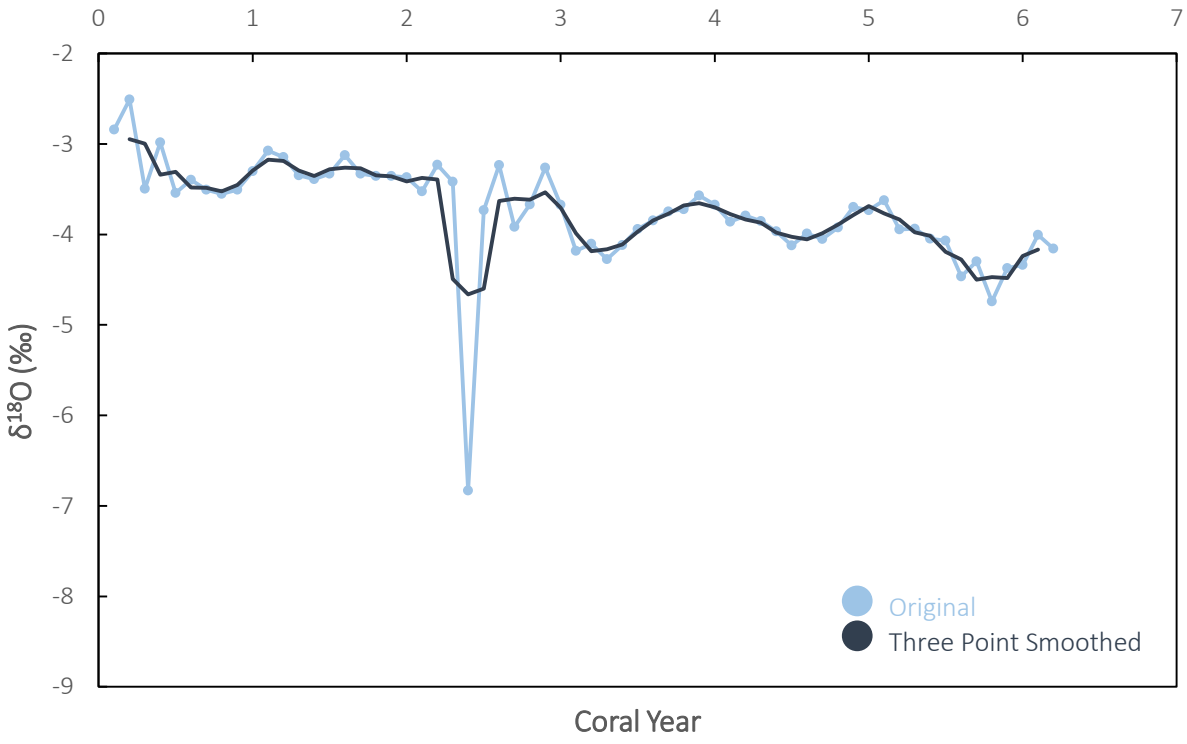


**Fig. 11:** $\delta^{18}O$ transect analysis of the Pleistocene coral BZRP14. A three-point smoothing analysis is superimposed on the raw data.

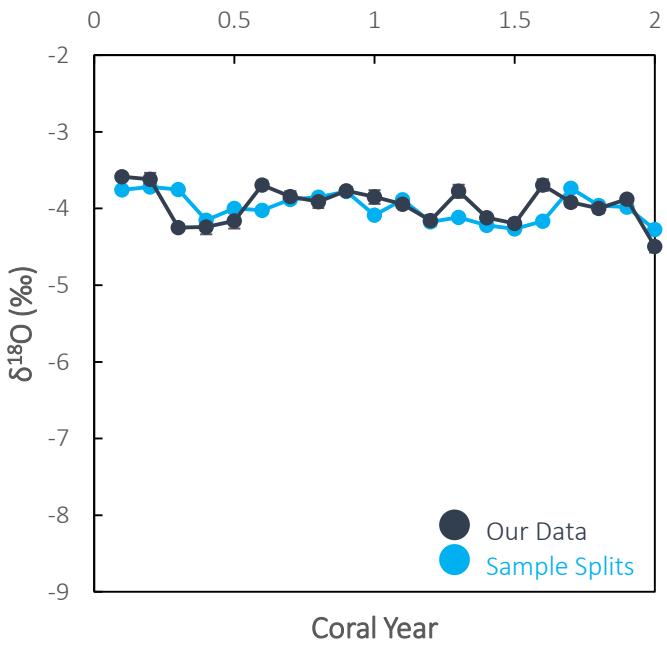


**Fig. 12:** $\delta^{18}O$ transect analysis of the modern coral BZ14RP. Two sets of data are shown, representing sample splits analyzed at Washington and Lee and the University of Miami.

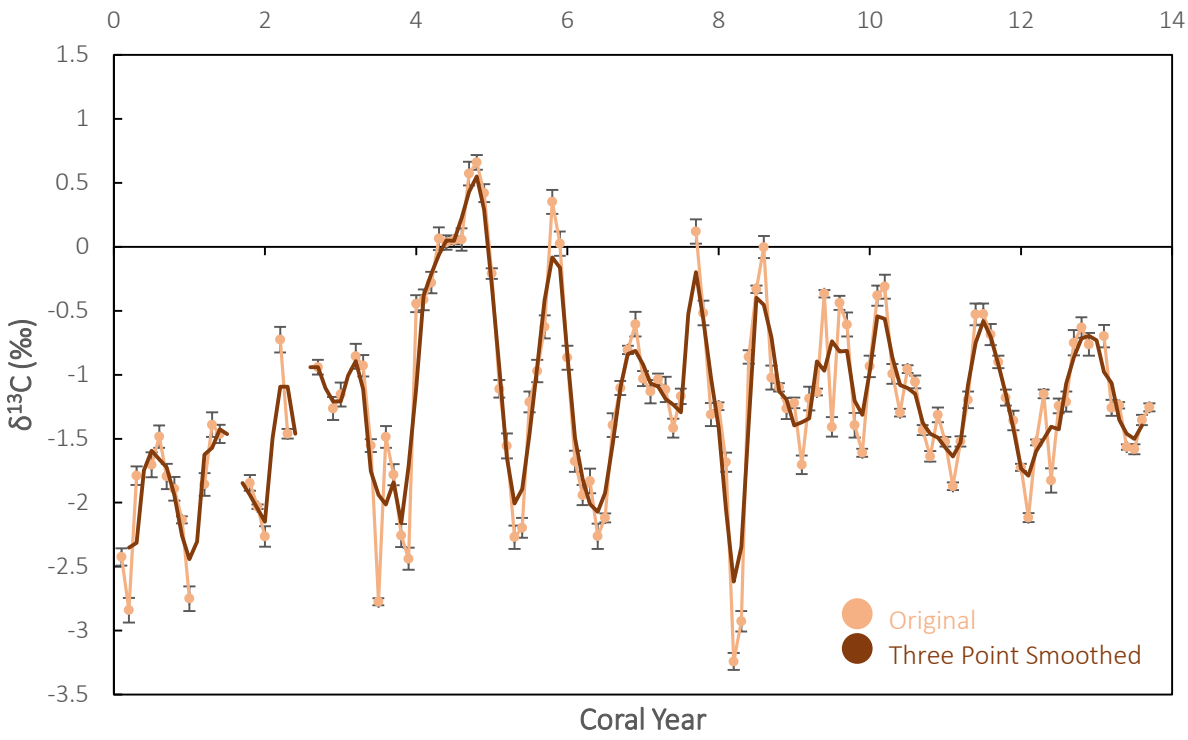


**Fig. 13:** $\delta^{13}C$ transect analysis of the Pleistocene coral BZRP12. A three-point smoothing analysis is superimposed on the raw data.

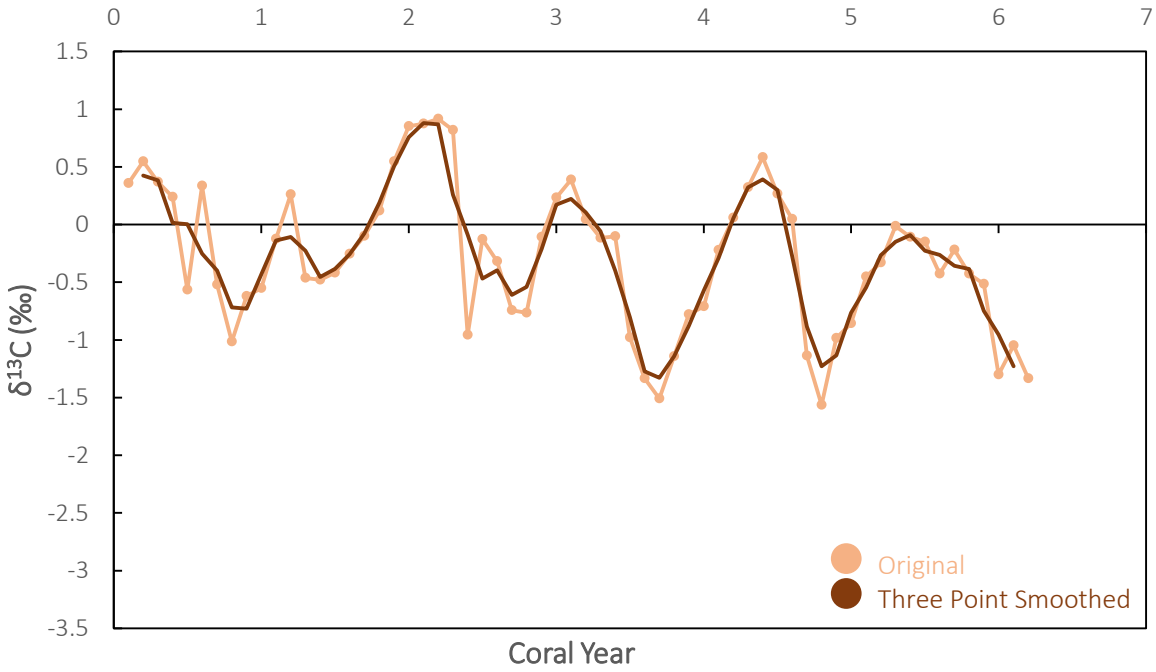


**Fig. 14:** $\delta^{13}C$ transect analysis of the Pleistocene coral BZRP14. A three-point smoothing analysis is superimposed on the raw data.

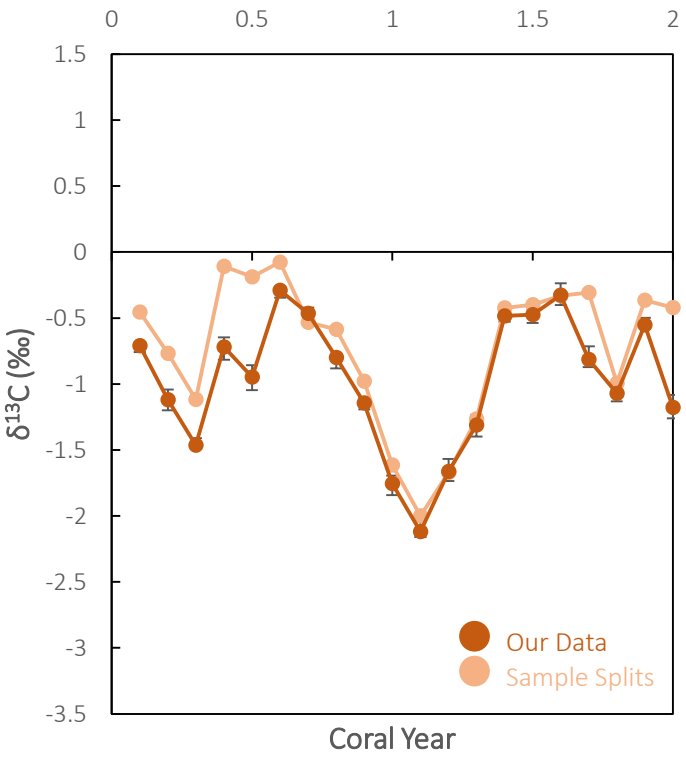


**Fig. 13:** $\delta^{13}C$ transect analysis of the modern coral BZ14RP. Two sets of data are shown, representing sample splits analyzed at Washington and Lee and the University of Miami.

## V. Discussion

The results of this study indicate that (1) seasonality differences are expressed in the geochemistry of our corals and (2) sampling resolution affects the amplitude of the seasonal range captured from one coral year. However, several uncertainties exist, namely the age uncertainties of the two Pleistocene corals, the contradiction between the isotopic variability of the Coral Gardens modern coral and the Rocky Point modern coral, and the species discrepancy between the Rocky Point modern coral and the Rocky Point Pleistocene corals.

The Pleistocene coral in this study was dated by two independent $^{234}U/^{230}Th$ analyses. In 2002, the Pleistocene coral (sample ID unknown) was dated at 128-124 Ka. The $^{234}U/^{230}Th$ dates generated in 2016 by Dr. Tara Clark place the Pleistocene coral (BZRP12 and BZRP17) at 135.3 ± 0.9 Ka and 131.2 ± 1.1 Ka using the Thompson open-system age model (Thompson et al., 2003). Although there is a discrepancy between these dates, we have chosen to use the 128-124 Ka dates obtained in 2002 for multiple reasons. The open-system modeling developed by Thompson et al., 2003 is still open to question and may not represent real-world situations (Clark, personal communication). Additionally, the Pleistocene terrace, where the fossil corals were retrieved, sits above sea level at an elevation consistent with MIS 5e elevation (Greer, personal communication).

The larger and more variable growth rate of the modern coral BZ14RP compared to the Pleistocene corals is most likely a function of the different growth natures between the two *Orbicella* subspecies. BZRP14 had a slightly larger mean growth rate but less variable growth rate than BZRP12. The modern coral BZ14RP showed the largest and most variable growth rate, which would be expected from a different subspecies of *Orbicella*.

Annually resolved data from the Pleistocene coral BZRP12 and the modern coral BZ14RP substantiate the idea that sampling at lower resolutions yields a reduced seasonal cycle, as compared with higher sampling resolutions (Leder et al., 1996). The seasonal ranges acquired at 4 samples per year were dampened compared to the seasonal ranges acquired at 10 samples per year. The $\delta^{18}O$ seasonal range

increased 1.81‰ from the lowest to the highest sampling resolution for BZRP12 and 0.58‰ for BZ14RP. The $\delta^{13}C$ seasonal range increased by 1.56‰ for BZRP12 and stayed the same for BZ14RP.

Paleotemperatures derived from the sampling resolution data (using the equation defined by Leder et al., 1996) support the hypothesis that a higher sampling resolution is more representative of the seasonal cycle of one coral year. At a resolution of 10 samples per year, the Pleistocene coral BZRP12 and the modern coral BZ14RP displayed seasonal ranges 9.05°C and 2.9°C greater than the seasonal range captured at 4 samples per year. If this study had used a sampling resolution of 4 samples per year instead of 10 samples per year, the maximum seasonal ranges would have been underestimated by a maximum of 9.05°C, if $\delta^{18}O$ reflected temperature alone.

The greater shift of BZRP12 at two different resolutions compared to the smaller shift of BZ14RP may be a function of the higher degree of geochemical variability of the Pleistocene coral compared to the modern coral, due to the fact that the former grew during a period of greater seasonality and the latter grew during a time of moderate seasonality. That is, since BZ14RP had a smaller seasonal range to begin with, we would expect to see less variability between the maximum seasonal amplitude recorded in the coral vs. the minimum seasonal amplitude recorded in the coral. Since BZRP12 had a larger seasonal amplitude recorded in a coral year, it would be easier to misrepresent its seasonal range magnitude.

Ten samples per year was the best resolution for this study for multiple reasons. This was the highest possible sampling resolution for the Pleistocene corals, given their dense growth bands as a function of low LER. Not only was it not physically feasible to sample more than 10 per year, a higher sampling resolution would have been less cost effective and less time effective. Although some studies use a higher annual sampling resolution, at a certain threshold sampling resolution does not enhance seasonal range results. The seasonal data captured in this study are of the highest resolution possible and therefore the most representative of the isotopic range per coral year.

Three of the corals from this study yielded three different seasonal range amplitudes. The modern coral BZ14RP showed a smaller $\delta^{18}O$ and $\delta^{13}C$ seasonal range than each of the Pleistocene corals, where the Pleistocene coral BZRP14 expressed a lower seasonal range than BZRP12. Orbital forcing, the main driver behind seasonal ranges, could explain this large difference between the Pleistocene corals and the modern coral, given the different orbital forcing parameters defining their respective growth ages.

Although both Pleistocene corals are dated at MIS 5e, the maximum temperature ranges of the two Pleistocene corals differed by 4.03°C. The moderate seasonality of the Pleistocene coral BZRP14 with respect to the other Pleistocene coral BZRP12 may be explained by two different growth ages. $^{234}U/^{230}Th$ dating places them in MIS 5e, but does not give a tighter constraint, leaving some room for age interpretation. The large seasonal range of BZRP12 is consistent with seasonal ranges of a mid-interglacial coral by Felis et al., 2004 and the moderate seasonal range of BZRP14 is consistent with seasonal ranges of an end-interglacial coral by Felis et al., 2015. Thus, seasonal range dampening observed in the Pleistocene coral BZRP14, as compared with the larger seasonality of the Pleistocene coral BZRP12, may indicate that the former grew at the end-interglacial and the latter grew at the mid-interglacial. The Pleistocene coral BZRP14's seasonal range exceeded the modern coral BZRP14's seasonal range by 1.89°C, still indicating a higher seasonality during the interglacial, but at a dampened magnitude than that of the Pleistocene coral BZRP12. The progression from enhanced seasonality at the mid-interglacial to weakened seasonality at the end-interglacial is most likely due to changing orbital forcing parameters towards the end-interglacial (Felis et al., 2015).

An important caveat to note is that this study assumes that $\delta^{18}O$ is solely a function of sea surface temperature, when calculating maximum temperature ranges. This does not account for the salinity effect from ITCZ oscillation. During periods of high seasonality, the ITCZ reaches a larger spatial extent, meaning that it introduces an influx of precipitation into the Belizean reef system during part of the year, but is absent during the rest of the year, creating more arid conditions at the study locality. During periods of low seasonality, the ITCZ isn't as mobile, meaning that Belize is covered by the ITCZ during the

majority of the year, so precipitation is more constant. Since ITCZ mobility contributes to the $\delta^{18}O$ of sea water, but we are assuming that $\delta^{18}O$ is only a reflection of temperature, our results may be less variable than what they should be.

The lighter bulk $\delta^{18}O$ signature of the Pleistocene corals compared with the heavier signature of the modern corals reaffirms that the last interglacial experienced warmer temperatures and increased precipitation. If BZRP14 is indeed younger than BZRP12, its lighter bulk $\delta^{18}O$ signature could represent a trend from cooler to warmer temperatures, going from the mid interglacial, to the end-interglacial, to the modern. If our assumptions about age are not true, there are other factors that could explain the bulk isotopic difference and seasonal cycle difference between the two Pleistocene corals. They could have formed in different sub-environments, been exposed to different storm patterns, or received different nutrient availability, amongst other considerations.

The bulk variability of the modern coral taken from Coral Gardens is similar to that of the two Pleistocene corals. This may be due to the fact that the Coral Gardens coral was taken from a different locality than were the other three corals. Coral Gardens, located to the south of Rocky Point, is a system of patch reefs in a back reef lagoonal setting of 4-8m water depth (Busch et al., 2015). Since it is located inland of the Mesoamerican barrier reef, it experiences more open marine circulation than Rocky Point (Greer, personal communication). The Rocky Point modern reef is located at the convergence of the Belizean coastline and the Mesoamerican barrier reef, which protects it from reef break (Greer, personal communication). The Rocky Point patch reefs today grow in very shallow (~2m water depth) water. The Pleistocene terrace at Rocky Point, where BZRP12 and BZRP14 were collected, represents a shallow water fringing reef that deepens seaward (Greer, personal communication).

Previous research has also demonstrated how corals can reflect insolation based climate in the Pleistocene (Suzuki et al., 2001, Felis et al., 2004; Al-Rousan et al., 2013; Felis et al., 2015, Winter et al., 2003). A Pleistocene-aged coral from the Pacific Ocean expressed a 10% greater seasonality for $\delta^{18}O$ and a 20% greater seasonality for $\delta^{13}C$ compared with a modern coral (Suzuki et al., 2001). The 5.92°C

difference between our Pleistocene and modern corals is remarkably greater than the 0.9°C difference reported from these Pacific corals (Suzuki et al., 2001). Pleistocene-aged corals from the Red Sea also recorded an augmented seasonality compared to modern records (Felis et al., 2004). Our results indicate a possible 10.7°C maximum temperature range during the last interglacial, whereas corals from the Pacific Ocean, the Red Sea, and the northeastern Caribbean yield only a 7.55°C, 8.4°C, or 5°C temperature range (Suzuki et al., 2001; Felis et al., 2004; Winter et al., 2003). Geochemistry of an end-interglacial coral from the southern Caribbean yields a seasonal temperature range of 2.4°C, which is 4.2°C lower than the seasonal temperature range obtained from our proposed end-interglacial coral BZRP14 (Felis et al., 2015).

In summation, oxygen isotope ratios are used as paleothermometers, which can support the aforementioned claims that (1) our corals express a difference in seasonal ranges between the Pleistocene and the modern and (2) that sampling resolution plays an important role in attaining the most representative seasonal amplitude. If $\delta^{18}O$ only represents temperature, the 5.92°C excess of the Pleistocene coral BZRP12 seasonal range over the modern coral BZ14RP seasonal range validates that Belize experienced a larger seasonal amplitude temperature and/or precipitation cycle during the Pleistocene epoch. The maximum seasonal paleotemperature change (if $\delta^{18}O$ reflects only temperature and no 'salinity' effect) calculated from our $\delta^{18}O$ data suggest that the maximum seasonal range in temperature of the modern coral was the lowest (4.7°C), BZRP14 geochemistry represented a larger seasonal range (6.6°C), and BZRP12 expressed the largest seasonal range (10.7°C).

## VI. Conclusions

Comparison of geochemical composition and linear extension rates between two Pleistocene corals and two modern corals from Belize indicates that the last interglacial experienced a larger seasonal range in temperature and/or precipitation than at present. These results are expected, given the increased summer insolation but decreased winter insolation acting on the Northern Hemisphere during the last interglacial. From smallest to largest, the modern coral BZ14RP had a mean seasonal temperature range of 4.7°C, followed by the Pleistocene coral BZRP14 at 6.6°C and then the Pleistocene coral BZRP12 at 10.7°C. From these data, we conclude that the Pleistocene showed a larger seasonality than the modern Rocky Point coral and that orbital forcing likely controls seasonality at low latitudes, as evidenced by the Caribbean corals from this study.

## VII. References


Al-Rousan, S., & Felis, T. (2013). Long-term variability in the stable carbon isotopic composition of porites corals at the northern gulf of aqaba, red sea. Palaeogeography, Palaeoclimatology, Palaeoecology, 381-382, 1-14.

Busch J, Greer L, Harbor D, Wirth K, Lescinsky H, Curran HA, de Beurs K, (in press) Quantifying exceptionally large populations of Acropora spp. corals off Belize using sub-meter satellite imagery classification. Bulletin of Marine Science. Vol 92, No 2. 2016

Corrège, T. (2006). Sea surface temperature and salinity reconstruction from coral geochemical tracers. Palaeogeography, Palaeoclimatology, Palaeoecology, 232(2-4), 408-428.

DeCorte, Ilian, & Wirth, Karl (2015). A record of environmental change in Caribbean coral reefs: sclerochronology and geochemistry of o. Faveolata as a paleoclimate proxy at Coral Gardens and Rocky Point, Belize. Unpublished manuscript.

Druffel, E. R. M. (1997). Geochemistry of corals: Proxies of past ocean chemistry, ocean circulation, and climate. Proceedings of the National Academy of Sciences of the United States of America, 94(16), 8354-8361.

Felis, T., Giry, C., Scholz, D., Lohmann, G., Pfeiffer, M., Pätzold, J., . . . Scheffers, S. R. (2015). Tropical atlantic temperature seasonality at the end of the last interglacial. Nature Communications, 6

Felis, T., Lohmann, G., Kuhnert, H., Lorenz, S. J., Scholz, D., Pätzold, J., . . . Al-Moghrabl, S. M. (2004). Increased seasonality in middle east temperatures during the last interglacial period. Nature, 429(6988), 164-168.

Gagan, M. K., Ayliffe, L. K., Beck, J. W., Cole, J. E., Druffel, E. R. M., Dunbar, R. B., & Schrag, D. P. (2000). New views of tropical paleoclimates from corals. Quaternary Science Reviews, 19(1-5), 45-64.

Grottoli, A. G. (2000). Stable carbon isotopes (δ 13C) in coral skeletons. Oceanography, 13(SPL.ISS. 2), 93-97.

Grottoli, A. G., & Eakin, C. M. (2007). A review of modern coral δ18O and Δ14C proxy records. Earth-Science Reviews, 81(1-2), 67-91.

Intertropical Convergence Zone: January-July. Digital image. Wikipedia. Wikimedia Foundation, n.d. Web. 13 Apr. 2016.

Kim, S.J., Lü, J. M., Yi, S., Choi, T., Kim, B. -., Lee, B. Y., . . . Kim, Y. (2010). Climate response over Asia/Arctic to change in orbital parameters for the last interglacial maximum. Geosciences Journal, 14(2), 173-190.

Kim, S.T., & O'Neil, J. R. (1997). Equilibrium and nonequilibrium oxygen isotope effects in synthetic carbonates. Geochimica et Cosmochimica Acta, 61(16), 3461–3475.

Kukla, G. J., Bender, M. L., de Beaulieu, J., Bond, G., Broecker, W. S., Cleveringa, P., . . . Winograd, I. J. (2002). Last interglacial climates. Quaternary Research, 58(1), 2-13.

Leder, J. J., Swart, P. K., Szmant, A. M., & Dodge, R. E. (1996). The origin of variations in the isotopic record of scleractinian corals: I. oxygen. Geochimica Et Cosmochimica Acta, 60(15), 2857-2870.

Linsley, B. K., Dunbar, R. B., Wellington, G. M., & Mucciarone, D. A. (1994). A coral-based reconstruction of intertropical convergence zone variability over central america since 1707. Journal of Geophysical Research, 99(C5), 9977-9994.

Maslin, M. A., & Brierley, C. M. (2015). The role of orbital forcing in the early middle pleistocene transition. Quaternary International, 389, 47-55.

McConnaughey, T. (1989). 13C and 18O isotopic disequilibrium in biological carbonates: I. patterns. Geochimica Et Cosmochimica Acta, 53(1), 151-162.

Merlis, T. M., Schneider, T., Bordoni, S., & Eisenman, I. (2013). The tropical precipitation response to orbital precession. Journal of Climate, 26(6), 2010-2021.

Ruddiman, W. F. Earth's Climate: Past and Future. New York: W.H. Freeman, 2001. Print.

Ruddiman, W. F. (2006). Orbital changes and climate. Quaternary Science Reviews, 25(23-24), 3092-3112.

Schneider, T., Bischoff, T., & Haug, G. H. (2014). Migrations and dynamics of the intertropical convergence zone. Nature, 513(7516), 45-53.

Suzuki, A., Gagan, M. K., De Deckker, P., Omura, A., Yukino, I., & Kawahata, H. (2001). Last interglacial coral record of enhanced insolation seasonality and seawater 18O enrichment in the Ryukyu Islands, Northwest Pacific. Geophysical Research Letters, 28(19), 3685-3688.

Swart, P. K. (1983). Carbon and oxygen isotope fractionation in scleractinian corals: A review. Earth Science Reviews, 19(1), 51-80.

Gas Bench II Operating Manual (2009). *Gas Bench II*. Thermo Fisher Scientific, Bremen, Germany.

Thompson, W. G., Spiegelman, M. W., Goldstein, S. L., & Speed, R. C. (2003). An open-system model for U-series age determinations of fossil corals. Earth and Planetary Science Letters, 210(1-2), 365-381.

Winter, A., Paul, A., Nyberg, J., Oba, T., Lundberg, J., Schrag, D., & Taggart, B. (2003). Orbital control of low-latitude seasonality during the Eemian. Geophysical Research Letters, 30(4), 12-1.